nature biomedical engineering

SUPPLEMENTARY INFORMATION

https://doi.org/10.1038/s41551-018-0257-3

In the format provided by the authors and unedited.

An intravascular magnetic wire for the high-throughput retrieval of circulating tumour cells in vivo

Ophir Vermesh[1,2,12], Amin Aalipour[1,2,3,12], T. Jessie Ge[1,2,4,12], Yamil Saenz[2], Yue Guo[5], Israt S. Alam[1,2], Seung-min Park[1,2], Charlie N. Adelson[6], Yoshiaki Mitsutake[7], Jose Vilches-Moure[8], Elias Godoy[8], Michael H. Bachmann[2,9], Chin Chun Ooi[10], Jennifer K. Lyons[6], Kerstin Mueller[2], Hamed Arami[1,2], Alfredo Green[7], Edward I. Solomon[6], Shan X. Wang[5,11] and Sanjiv S. Gambhir[1,2*]

[1]Molecular Imaging Program at Stanford, Stanford University, Stanford, CA, USA. [2]Department of Radiology, Stanford University School of Medicine, Stanford, CA, USA. [3]Department of Bioengineering, Stanford University, Stanford, CA, USA. [4]Howard Hughes Medical Institute, Chevy Chase, MD, USA. [5]Department of Electrical Engineering, Stanford University, Stanford, CA, USA. [6]Department of Chemistry, Stanford University, Stanford, CA, USA. [7]Division of Cardiovascular Medicine, Stanford University, Stanford, CA, USA. [8]Department of Comparative Medicine, Stanford University, Stanford, CA, USA. [9]Department of Pediatrics, Stanford University, Stanford, CA, USA. [10]Department of Chemical Engineering, Stanford University, Stanford, CA, USA. [11]Department of Materials Science and Engineering, Stanford University, Stanford, CA, USA. [12]These authors contributed equally: Ophir Vermesh, Amin Aalipour, T. Jessie Ge. *e-mail: sgambhir@stanford.edu

Supplementary Information

Supplementary Figures

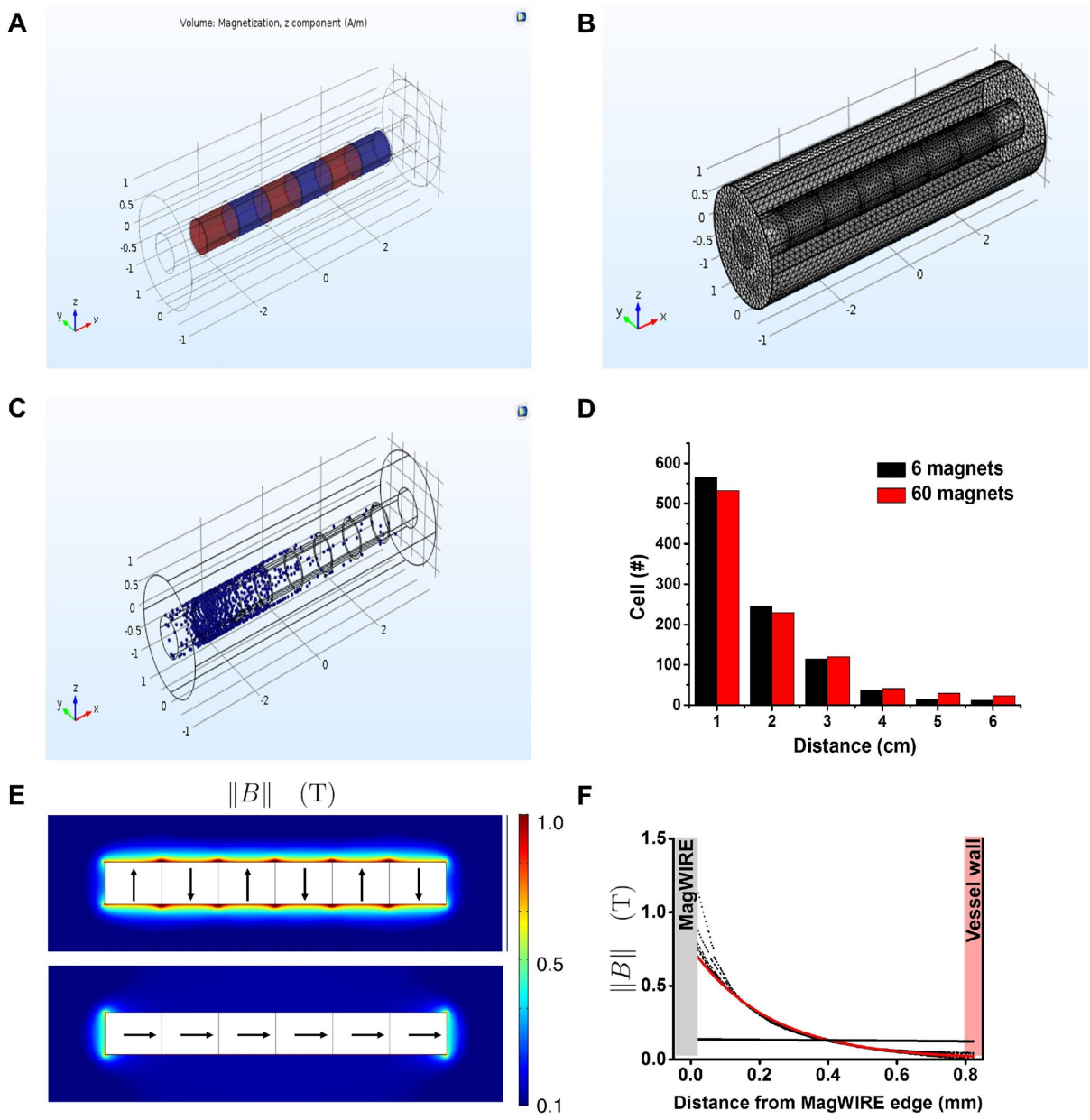

Figure S1. Numerical simulations of a MagWIRE segment. **(A)** The MagWIRE was modeled as repeating solid cylindrical units within a sheath. Each unit was assigned a magnetization such that the polarities alternated in the z-axis across the unit diameter. The vessel was modeled as a

magnetically insulating surface, and the volume between the vessel wall and the sheath was modeled as blood. **(B)** The complete mesh consists of 260308 elements for the geometry with 6 magnets. The element sizes for the blood volume and magnetic units were set to fine and extra fine, respectively. **(C)** We modeled 1000 magnetic particles (blue) in laminar flow at 2 cm/s past the MagWIRE with the Particle Tracing for Fluid Flow module (**Vid. S1**). The particles were modeled to bounce when contacting the outer wall of the vessel and to stick when contacting with the sheath, due to the strength of the magnetic interactions. 987 out of 1000 magnetically labeled cells were captured. **(D)** The 60-unit MagWIRE used in experiments was simplified to 6 units *in silico* to reduce computational load, and the particle velocity was scaled down 10-fold accordingly to 0.2 cm/sec. Compared to a simulation with 60 units, the simplified model gave a similar distribution of cells captured along the MagWIRE's length. (**E**) The magnetic flux density B is compared between different magnetic orientations (black arrows). The alternating orientation (top) has a much more uniform distribution of flux density along the entire length, while the axial orientation (bottom) only localizes flux density at the ends. **(F)** The magnetic flux density decays radially outward from the MagWIRE edge. Multiple points are sampled along the length of the magnet (dots), and the fit is shown (solid line). The surface flux density of the alternating polarity configuration (red) is much greater than that of the axial configuration (black).

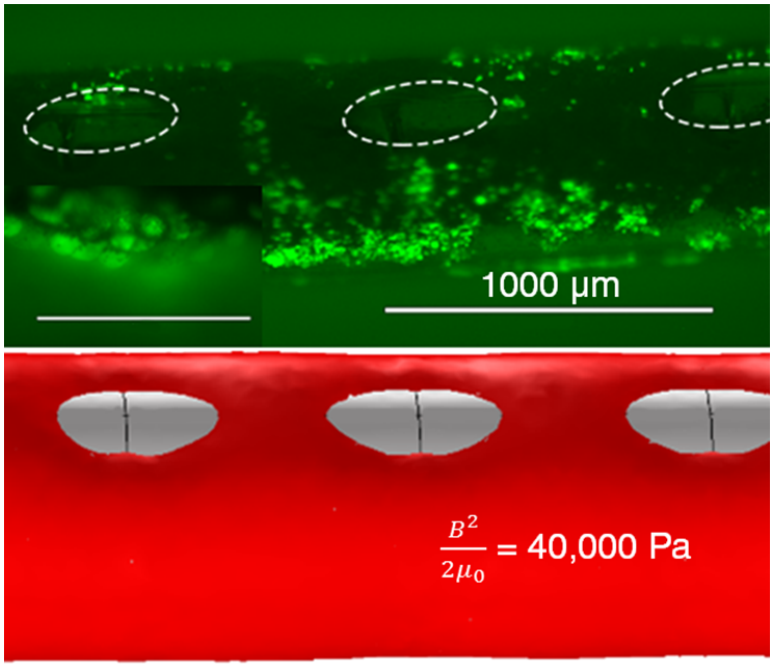

Figure S2. Distribution of captured cells on the MagWIRE: experiment vs. simulation.

The MagWIRE captured 4T1 cells which were transfected with GFP and EpCAM. Fluorescent microscopy (**top**) again reveals patterns of surface deposition of MPs and MP-labeled cells that agree with simulations (**bottom**) of surfaces of constant magnetic energy density. The dotted circles enclose exposed areas of the MagWIRE not coated with MPs or cells. **Top, inset**: Zoom in view of captured fluorescent cells at 40X magnification. Scale bar = 100 µm.

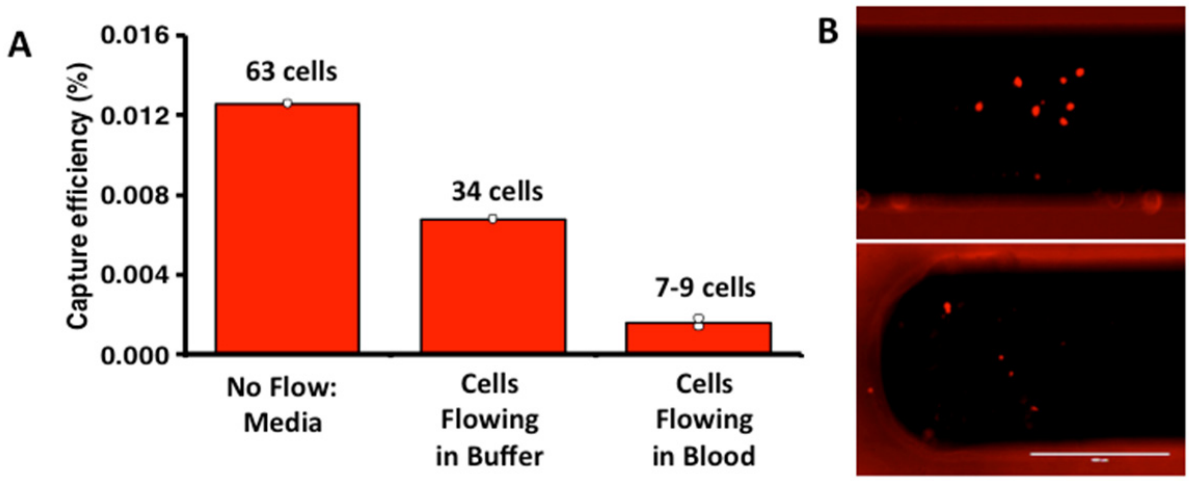

Figure S3. Capture efficiency of model CTCs by Gilupi CellCollector® in flow. (A) The Gilupi CellCollector was exposed for 30 minutes to a solution containing ~5×10^5 fluorescently-stained H1650 cells in cell culture media in a 2-mL tube with gentle rocking (as per vendor protocol), and to 5 mL of buffer or blood containing ~5×10^5 cells flowing at 2cm/sec in a closed-loop system. The total number of cells captured is listed above each bar (n=2 independent experiments for cells in flowing blood). (B) Representative microscopy images of fluorescently-stained H1650 cells bound to the CellCollector after incubation under no-flow conditions (top) and flowing blood (bottom), as detailed in (A). Compare with cell coverage of MagWIRE under similar conditions (Fig. 3D). Scale bar = 400 μm.

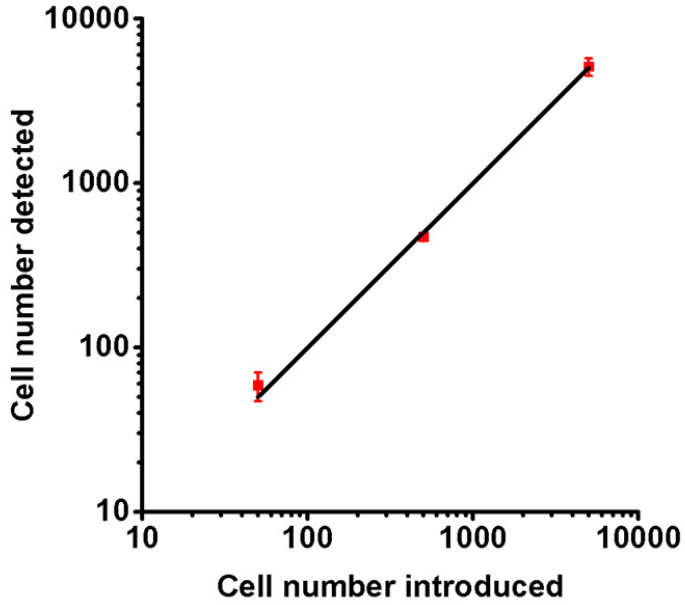

Figure S4. Effect of MP labeling on cell quantification by PCR. MP-labeling of cells does not interfere with quantification by qPCR (red, $y = 0.97x + 0.11$), when compared to standards of unlabeled cells (black, $y = x$) (n=3 independent samples).

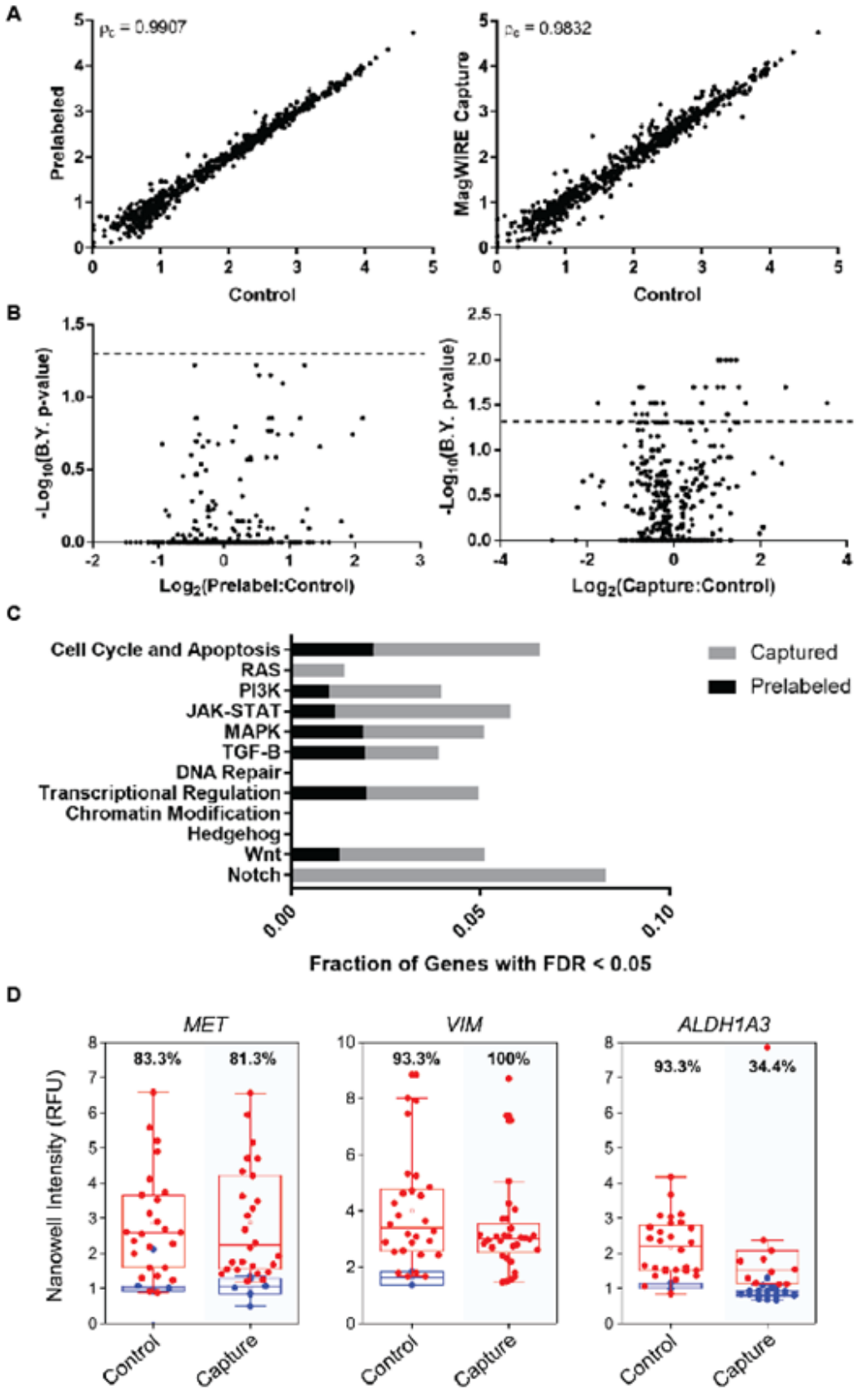
A
ρ_c = 0.9907
Prelabeled
Control
ρ_c = 0.9832
MagWIRE Capture
Control
B
-Log10(B.Y. p-value)
Log2(Prelabel:Control)
-Log10(B.Y. p-value)
Log2(Capture:Control)
C
Cell Cycle and Apoptosis
RAS
PI3K
JAK-STAT
MAPK
TGF-B
DNA Repair
Transcriptional Regulation
Chromatin Modification
Hedgehog
Wnt
Notch
Captured
Prelabeled
0.00
0.05
0.10
Fraction of Genes with FDR < 0.05
D
MET
VIM
ALDH1A3
Nanowell Intensity (RFU)
83.3%
81.3%
93.3%
100%
93.3%
34.4%
Control
Capture
Control
Capture
Control
Capture

Figure S5. Transcriptomic analysis of magnetically labeled and MagWIRE captured cells. (**A)** Plots of log-transformed, normalized gene expression sets for unperturbed (control) vs. experimental conditions (prelabeled, MagWIRE capture) with respective concordance correlation coefficients. **(B)** Volcano plots depicting relative fold-changes of gene expression against significance level. Dashed line signifies a Benjamini-Yekutieli p-value (false discovery rate) of 0.05. **(C)** Plot of the fraction of statistically significant gene expression alterations that are implicated in various cancer-associated pathways for both prelabeled and MagWIRE captured cells. **(D)** Single-cell gene expression analysis of VIM, ALDH, and MET expression using the Nanowell device shows similarity in expression profiles for VIM and MET with downregulation of ALDH potentially in response to cell stress. Expression levels are shown in relative fluorescence units of each individual well, as detailed in prior work[1]. Cells shown in blue did not meet the algorithmic criteria as described in Park et al. for sufficient expression of the particular gene. Percentages represent the fraction of analyzed cells in the cohort that expressed the given gene. Minima = 5th percentile, maxima = 95th percentile, center = median, and box extends from the 25th to 75th percentile. n=3 independent runs for control and capture experiments.

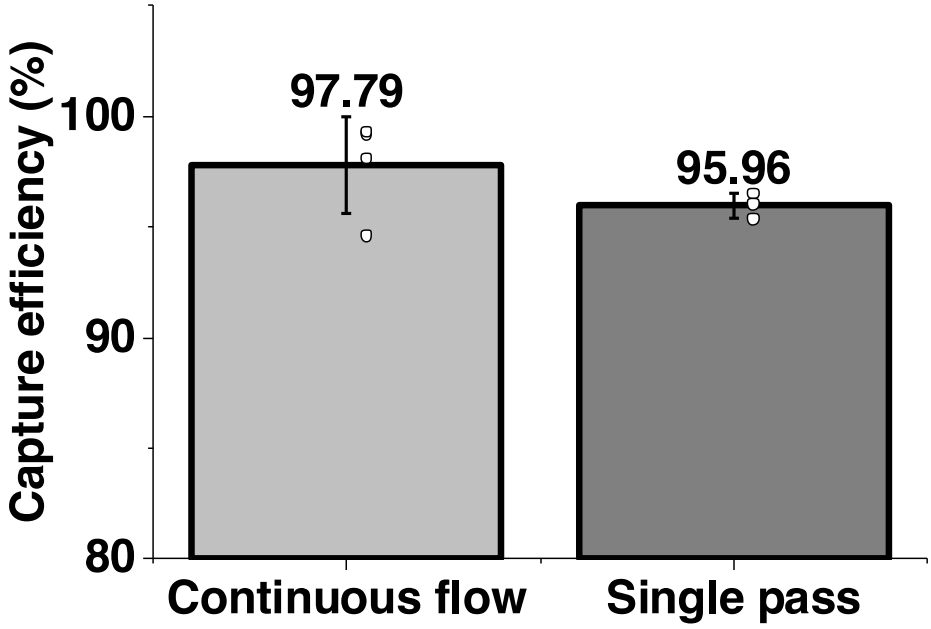

Figure S6. Capture Efficiency of MPs by the MagWIRE. The vast majority of MPs (>95%) introduced into the system are captured by the MagWIRE, even on the first pass. MPs were quantified as follows: after postlabeling experiments in buffer, the fluid was emptied into a reservoir for UV-Vis analysis of MP concentration. The absorbance at 660 nm was compared to standards of anti-EpCAM Dynabeads ranging from 12.5 μg/mL to 100 μg/mL. Mean ± SE, n=3 independent experiments.

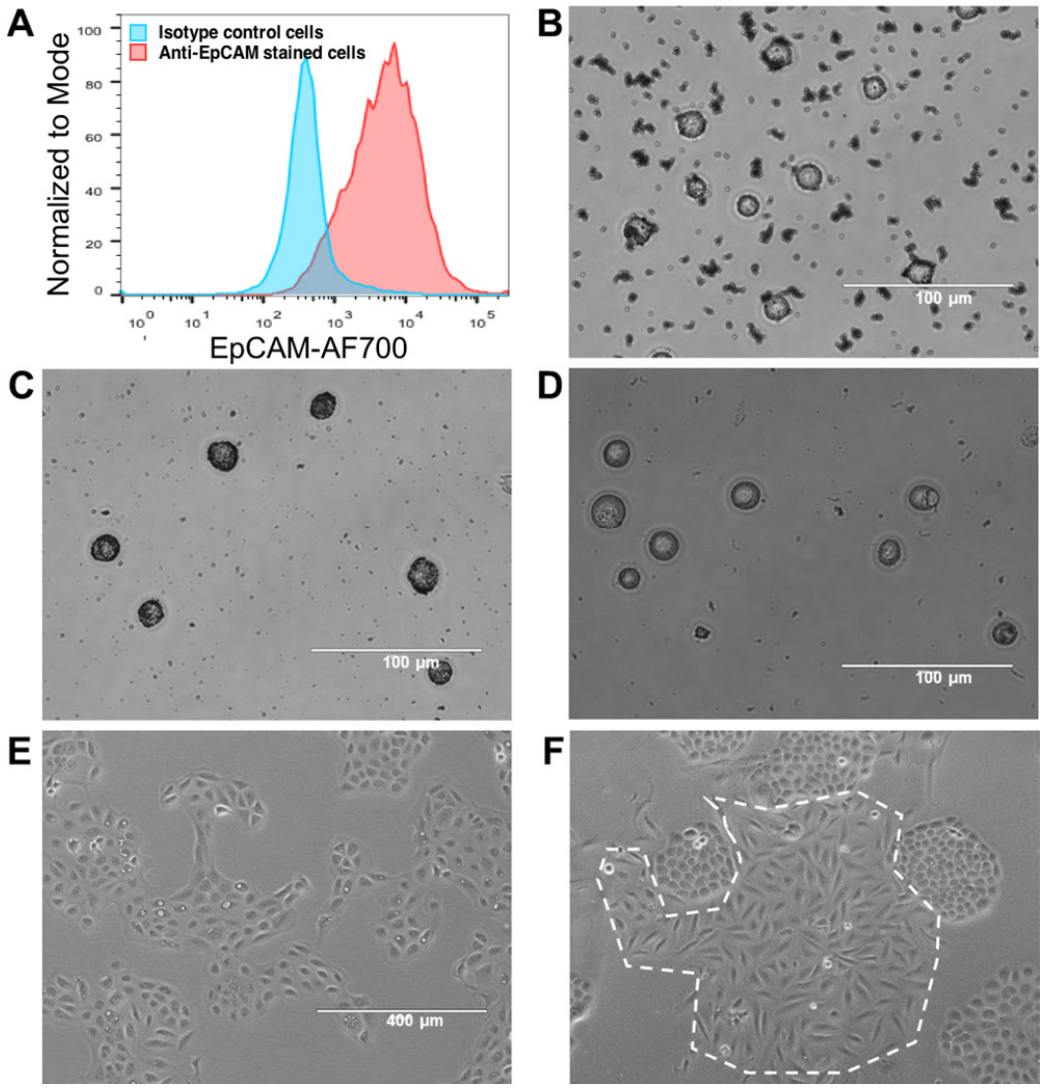

Figure S7. Effect of H1650 cells' EpCAM surface expression on MP labeling and cell capture. (A) Flow cytometry of H1650 cells shows a wide range of EpCAM expression across cells within a single passage. **(B)** Microscopy of prelabeled cells reflects similar variability in labeling by anti-EpCAM MPs. **(C)** H1650 cells postlabeled and captured in single pass flow displayed dense MP labeling, while (**D**) uncaptured cells showed little to no MP labeling. (**E**) Compared to H1650 cells at passage 3, cells at passage 10 **(F)** have a greater population of cells with a mesenchymal phenotype (dotted outline), known to be associated with EpCAM downregulation.

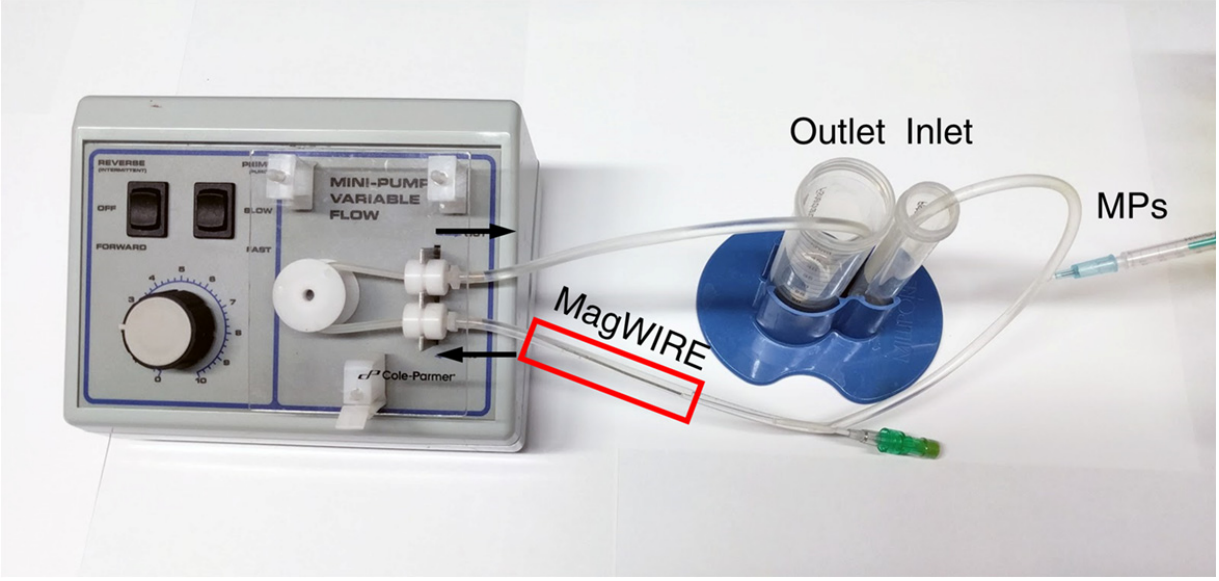

Figure S8. *In vitro* circulation system modified for single flow local enrichment. The inlet and outlet reservoirs are separate, and MPs are infused through a second catheter approximately 15 cm upstream of the beginning of the MagWIRE.

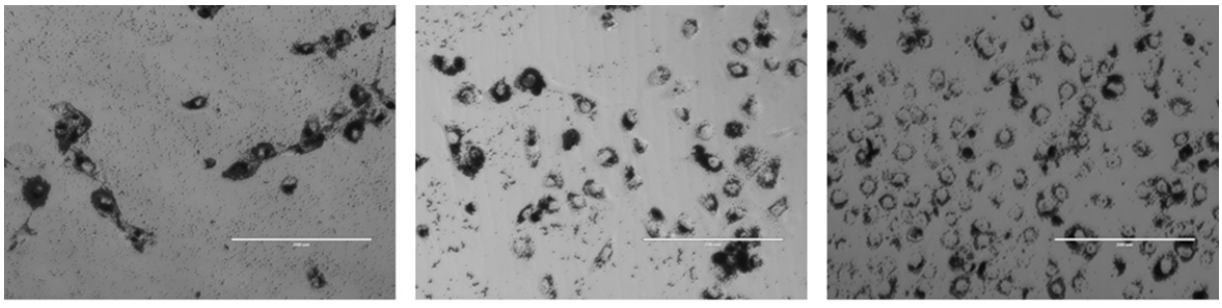

Figure S9. Captured MP-labeled cells propagate in cell culture. H1650 cells postlabeled with anti-EpCAM MPs in blood were captured and eluted for cell culture. As cells divide, there is a progressive decrease in the degree of MP-coating. Residual magnetic beads are washed after cell adhesion to the dish (after 24 hours).

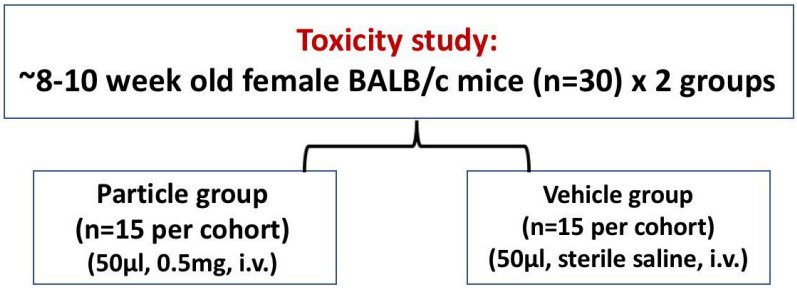

Time point	Cohort 1				Cohort 2
	Vitals	Feces/ Urine	CBC	Necropsy (histology, biodistribution)	Chem-electrolyte panel
Pre-injection	✔	✔	✔	✔	✔
Immediately post	✔				
24 hours	✔	✔	✔	✔	✔
1 week	✔	✔	✔	✔	✔
1 month	✔	✔	✔	✔	✔

n=5 per measurement for each timepoint

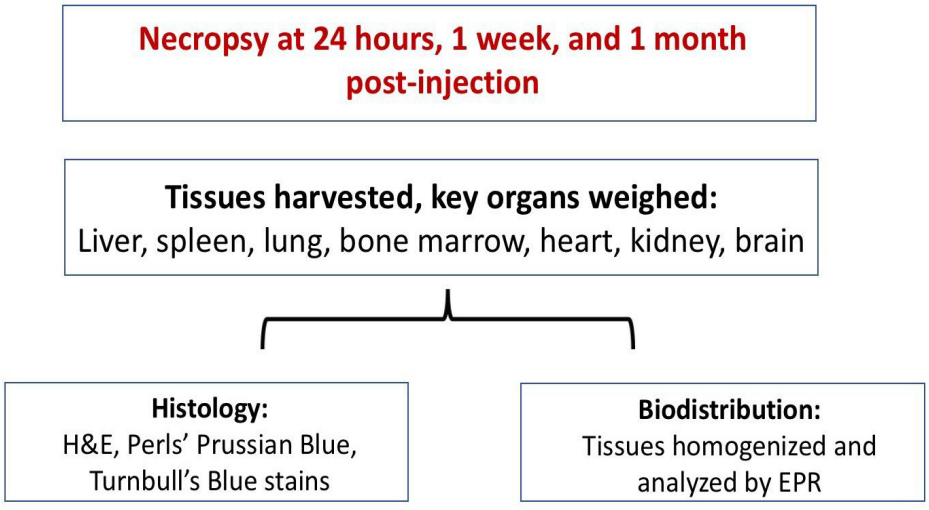

Figure S10. Toxicity study experimental design.

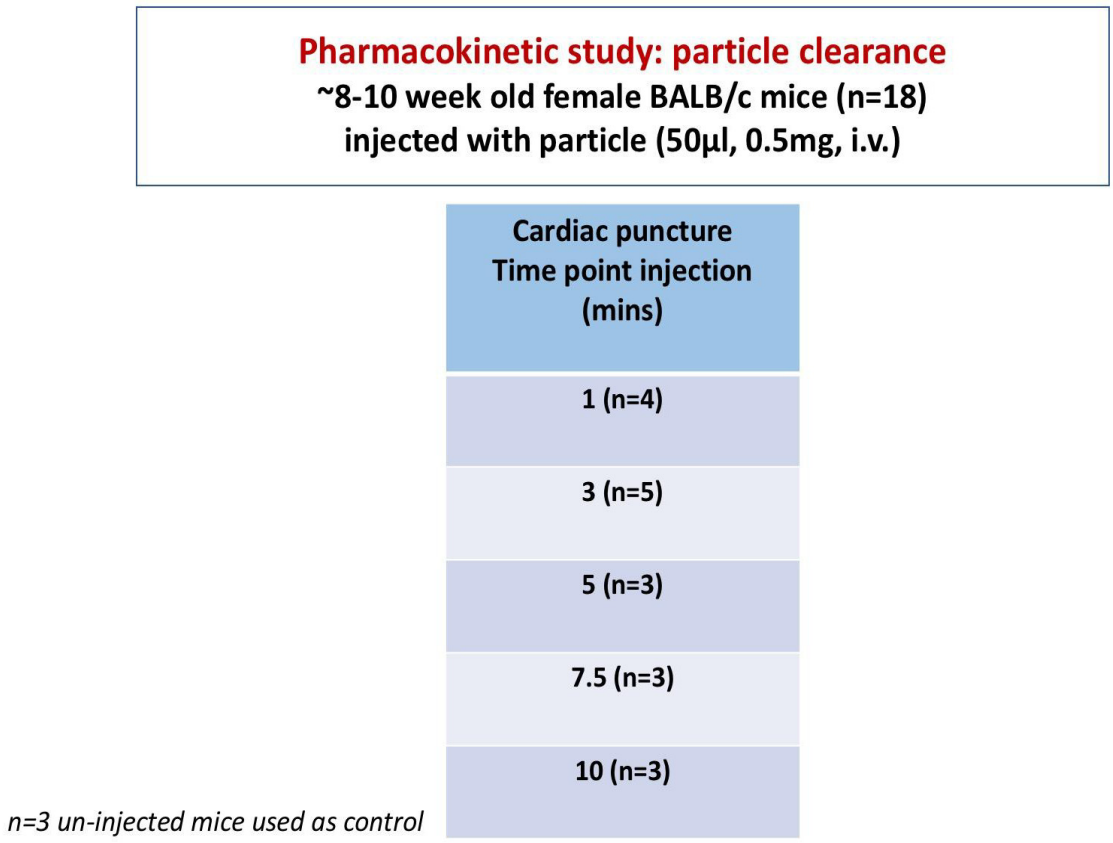

Figure S11. Pharmacokinetic study experimental design.

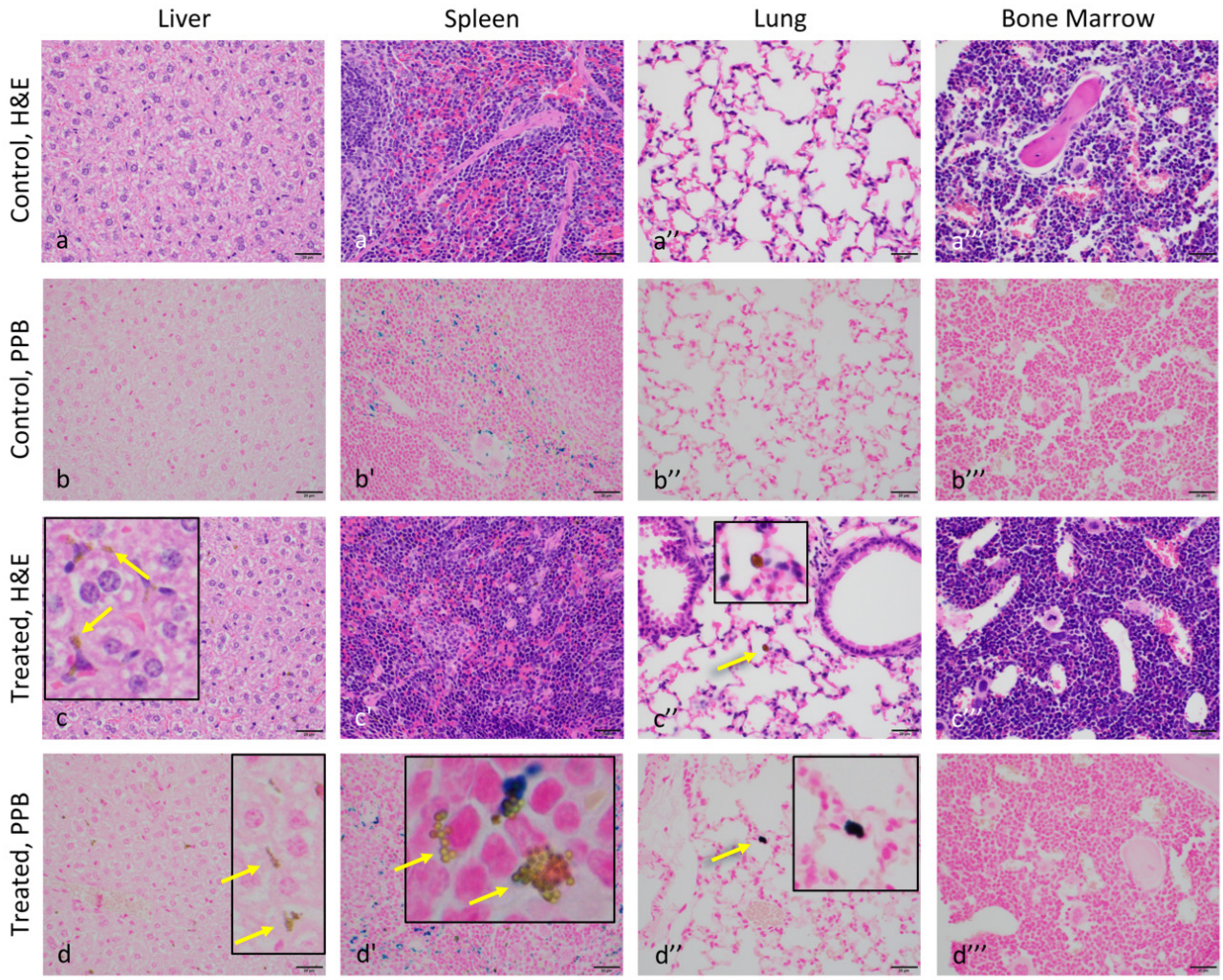

Figure S12. Histologic Assessment. Comparison of liver, spleen, lung, and bone marrow histology between vehicle-treated (**a-b'''**) and particle-treated (**c-d'''**) animals. (**a-a''', c-c''')** Hematoxylin and eosin (H&E). (**b-b''', d-d''')** Perls' Prussian Blue stain (PPB). Yellow arrows point to clusters of uniformly sized, round spherical bodies consistent with MPs. Insets show zoomed-in views of particle clusters. Magnification = 40x. Scale bar = 20 μm.

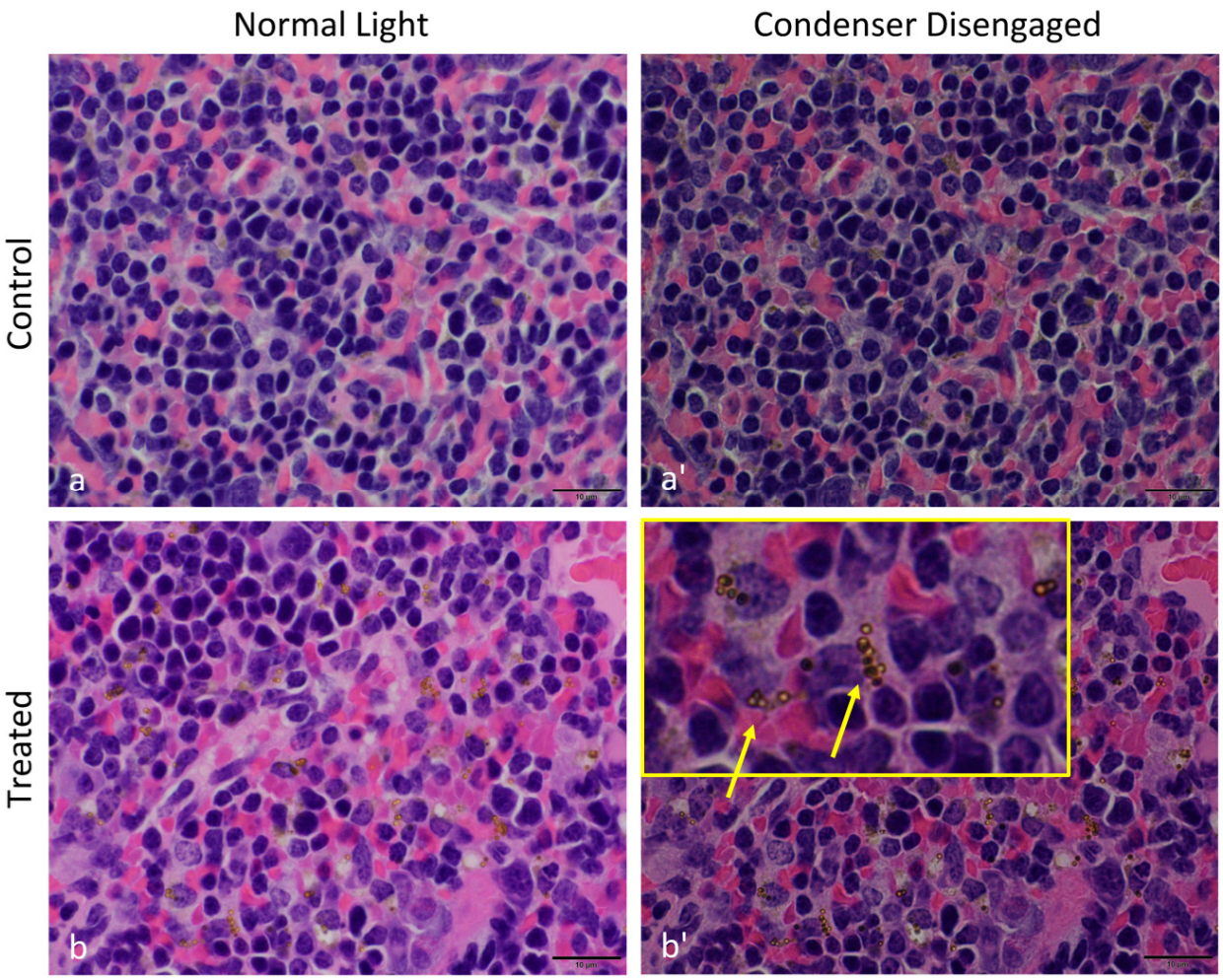

Figure S13. Spherical bodies accumulating in the spleens of particle-treated animals are distinct from hemosiderin deposits in hematoxylin and eosin stains. **(a-a')**: In spleens of vehicle-treated animals, there are amorphous brown deposits consistent with hemosiderin **(a)** that are not refractile **(a')**. **(b-b')**: In spleens of particle-treated animals, there are both amorphous brown deposits (consistent with hemosiderin) and spherical bodies **(b)**. The amorphous material consistent with hemosiderin is not refractile; however, the spherical bodies are refractile, which is enhanced when the microscope condenser is disengaged **(b')**. Magnification = 100x. Scale bar = 10 µm.

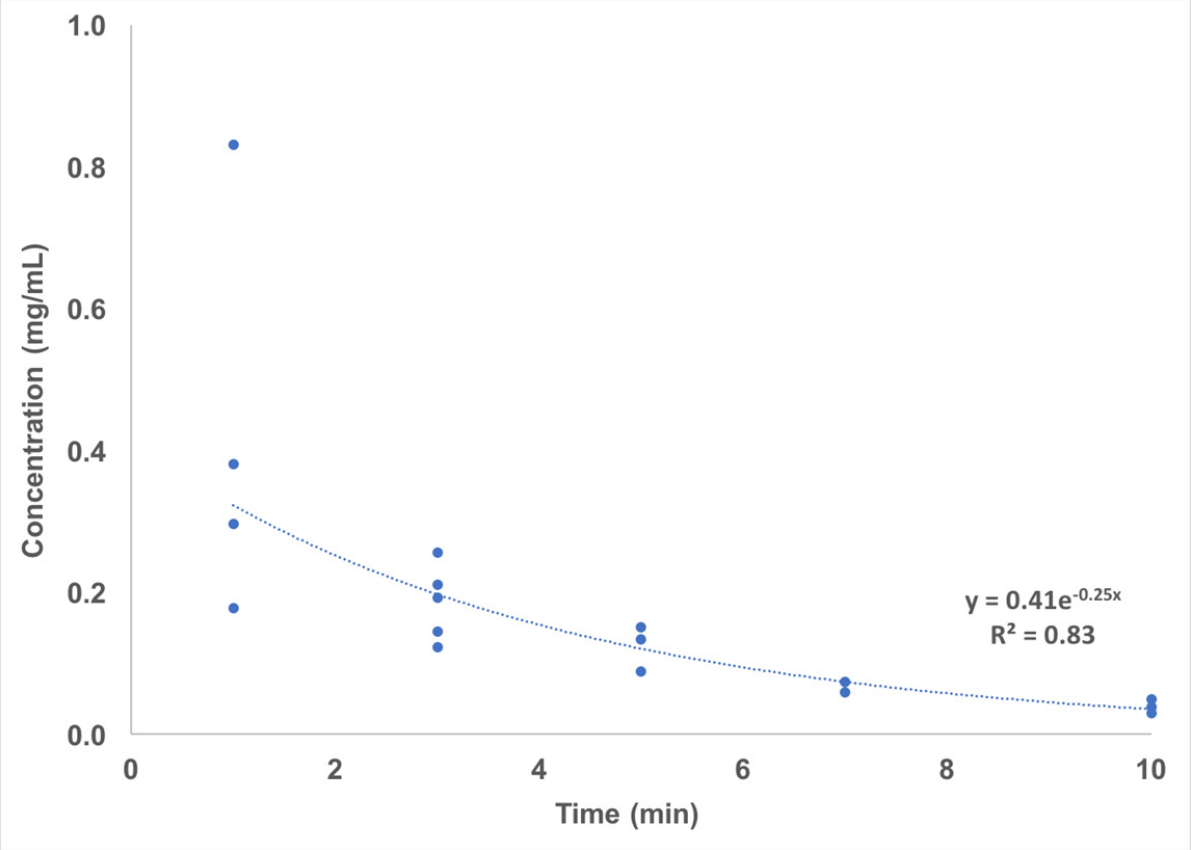

Figure S14. Blood half-life of anti-EpCAM conjugated 1 µm Dynabeads in mice. Blood was collected by terminal cardiac puncture over a range of time points from 1 to 10 minutes post-injection of 0.5mg MPs: t = 1, 3, 5, 7.5, and 10 mins (n=4, 5, 3, 3, and 3 independent samples, respectively). Blood from non-injected control mice was also collected (n=3 independent samples). Electron paramagnetic resonance (EPR) analysis was used to determine blood MP concentrations at each time point. Based on the best-fit curve, the blood half-life of MPs is ~2.8 minutes in mice. At this rate, ~97% of MPs would be cleared from the blood within ~15 minutes after injection.

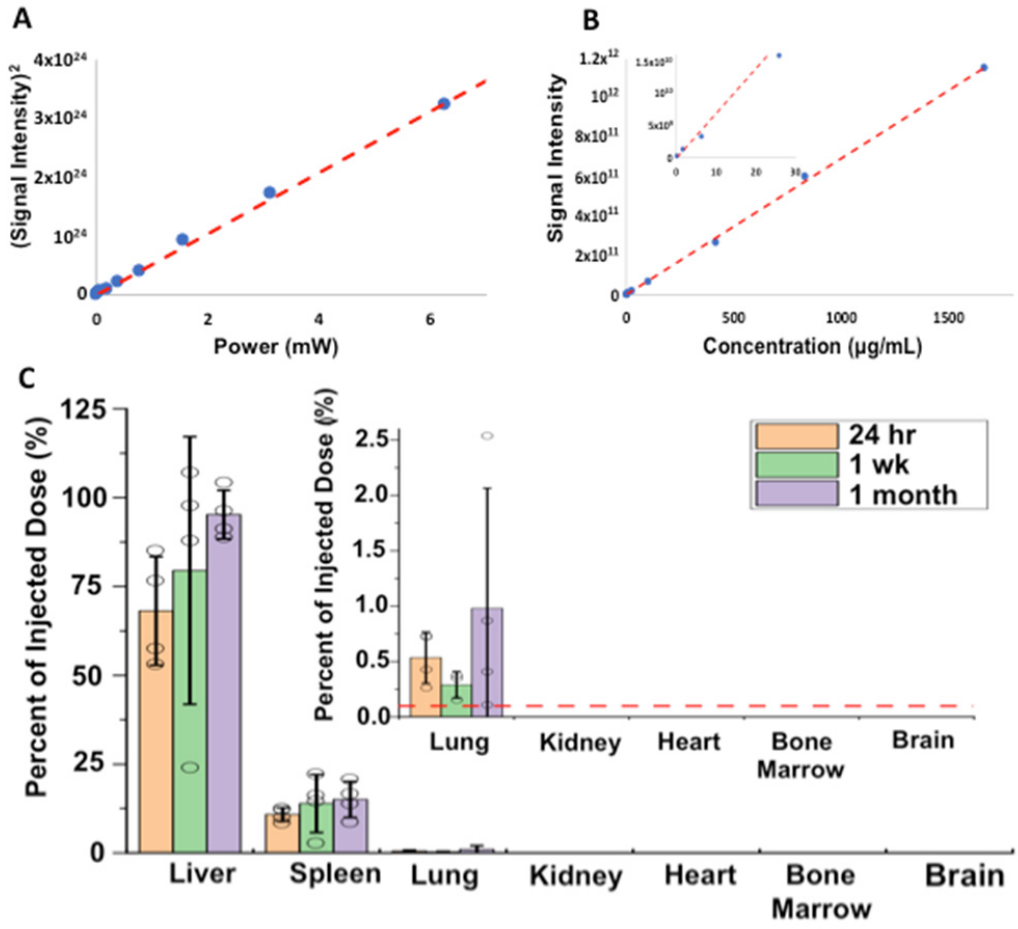

Figure S15. MP biodistribution in mice. (A) Square of EPR signal intensity versus microwave power for an MP quantity equivalent to the injected dose (0.5 mg) and suspended in 0.3 mL of buffer (1.67 mg/mL final concentration). First order fit shows that saturation does not occur below microwave powers of 6 mW. **(B)** EPR signal intensities versus nanoparticle concentration. First order fit shows that signal is linearly proportional to nanoparticle concentrations between 1670 and 0.20 µg/mL. **(C)** Percent injected dose of anti-EpCAM MPs in mouse organs harvested at 24 hours, 1 week, and 1 month (mean ± SE, n=5 biologically independent mice per time point) based on EPR measurements of tissue homogenates. Dotted red line in subplot indicates upper limit on minimum detectable concentration. MP levels in urine and feces were also below the detectable level. No MPs were detected in organs from vehicle-treated mice.

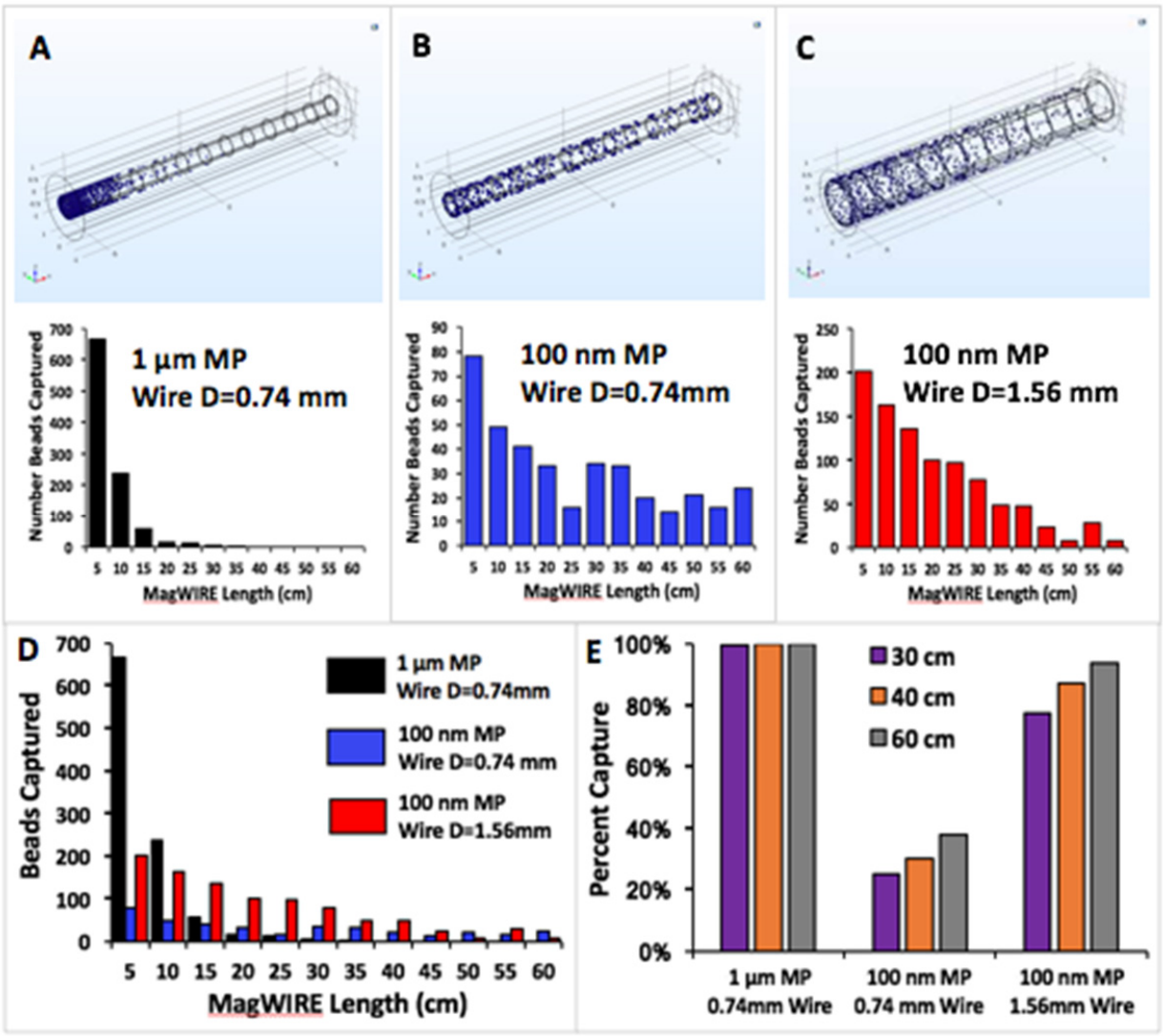
A
B
C
Number Beads Captured
1 µm MP
Wire D=0.74 mm
100 nm MP
Wire D=0.74mm
100 nm MP
Wire D=1.56 mm
MagWIRE Length (cm)
D
Beads Captured
1 µm MP
Wire D=0.74mm
100 nm MP
Wire D=0.74 mm
100 nm MP
Wire D=1.56mm
MagWIRE Length (cm)
E
Percent Capture
30 cm
40 cm
60 cm
1 µm MP
0.74mm Wire
100 nm MP
0.74 mm Wire
100 nm MP
1.56mm Wire

Figure S16. Computational comparison of capture efficiency for 1 μm Dynabeads and 100 nm MagSense MPs. Computational simulations were performed in which 1000 MPs were released at a blood velocity of 2 cm/sec. Histograms show the number of particles captured by the MagWIRE at various intervals along the wire on a single pass. **A**) Capture of 1 μm Dynabeads (Ms= 23.5 emu/g, density = 1.7 g/cm^3) with the same MagWIRE diameter (0.74 mm) as in the cell capture experiments. **B**) Capture of 100 nm MagSense MPs (Ms = 60 emu/g, density = 2.5 g/cm^3) with the same wire. **C**) Capture of 100 nm MagSense MPs using a thicker wire (1.56 mm diameter). **D**) Histograms from A-C are plotted on the same scale for comparison. E) Percent recovery of MPs in A-C at wire lengths of 30 cm, 40 cm, and 60 cm. Without changing the MagWIRE's diameter, single-pass capture efficiencies of 20-30% are possible for 100 nm MagSense beads at practical wire lengths (30-40 cm). With long-circulating MPs, capture efficiencies can be increased further by increasing the intravascular dwell time of the wire, as MPs can circulate past the wire repeatedly.

Video Captions

Video S1. Trajectories and distribution of magnetic particles along the MagWIRE. An animation plotting the trajectories and eventual distribution of magnetic particles along the MagWIRE was created by solving for the particle trajectories at 0.5 second intervals over a 2 second period.

Video S2. Magnetic particle accumulation on MagWIRE. Video depicts magnetic particles (injected from the right side) depositing on MagWIRE during a single pass by the MagWIRE. Similar to the simulation predictions, beads initially coat the proximal region of the MagWIRE and eventually coat the entire length of the wire.

Video S3. Single-pass method of rapid cell labeling and immediate capture. An animation describing the single-pass method of rapid cell labeling and immediate capture. MPs are injected directly upstream of the MagWIRE, such that circulating CTCs pass through a local area of high MP concentration for labeling and downstream capture.

Video S4. The porcine ear is highly vascularized. The porcine ear can be highly vascularized, with many collaterals branching off from the auricular vein. In such situations, many infused cells and MPs will flow through collaterals and never contact the MagWIRE.

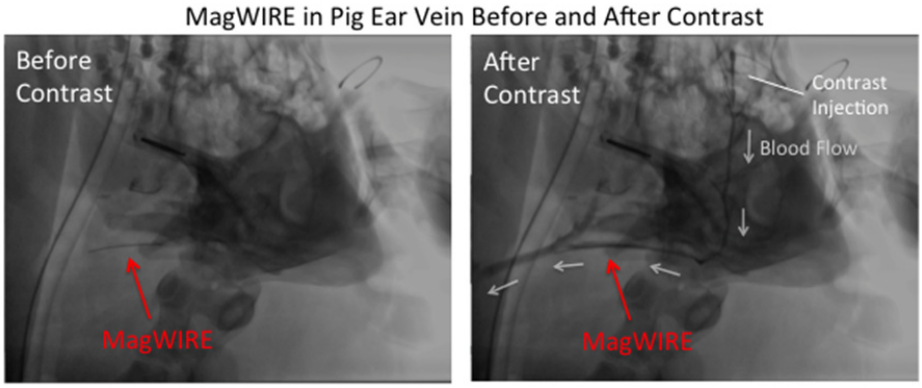

Video S5. Fluoroscopy image of the MagWIRE in a pig ear vein. Fluoroscopy view of MagWIRE situated within pig ear vein before (top left) and after (top right) iodinated contrast injection. Blood flow direction is indicated by white arrows. Clips are used to minimize collateral flows. Blood steadily flows unobstructed past the wire.

Supplementary Tables

Parameter	Value
Geometry	
Number of magnets	6
Vessel size	2.38 [mm]
Sheath diameter	0.8382 [mm]
Magnet	
Magnet diameter	0.7366 [mm]
Magnet length	0.9906 [mm]
Magnet remanence	1.4 [T]
Magnet coercivity	860 [kA/m]
Dynabead	
Dynabead diameter	1 [μm]
Dynabead density	1.7 [g/cm^3]
Dynabead mass magnetic susceptibility	0.00081 [m^3/kg]
Cell	
Cell diameter	25 [μm]
Dynabead per cell	100
Blood	
Blood viscosity = 40% hematocrit	0.0035 [Pa·s]
Flow rate	2 [cm/s]
Magnitude of magnetic field gradient: Frobenius norm $\| \nabla B \|_F$	
$\sqrt{(\frac{\partial B_x}{\partial x})^2 + (\frac{\partial B_y}{\partial x})^2 + (\frac{\partial B_z}{\partial x})^2 + (\frac{\partial B_x}{\partial y})^2 + (\frac{\partial B_y}{\partial y})^2 + (\frac{\partial B_z}{\partial y})^2 + (\frac{\partial B_x}{\partial z})^2 + (\frac{\partial B_y}{\partial z})^2 + (\frac{\partial B_z}{\partial z})^2}$	
Magnetophoretic force on superparamagnetic particles	
$\vec{F}_m = \frac{V}{\mu_0}\chi(\|H\|)(\vec{B}\cdot\nabla)\vec{B}$ where B is the magnetic flux density, μ_0 is the permeability of free space, and V is the particle volume. Based on the nonlinear M-H curve of the Dynabeads, a field dependent susceptibility $\chi(\|H\|)$ can be described by the equation: $\chi(\|H\|) = \frac{M_S}{\|H\|} L(\frac{3\chi_0 \|H\|}{M_S})$ where M_S is the saturation magnetization, χ_0 is the maximum volumetric susceptibility at low fields, and L(x) is the Langevin function $L(x) = \coth(x) - 1/x$.	

Table S1. COMSOL modeling parameters for MagWIRE simulations.

		Particle		Vehicle		Particle		Vehicle	
		Baseline	Post (t=0)	Baseline	Post (t=0)	Baseline	24 hours	Baseline	24 hours
MAP	(mmHg)	112 ± 5	107 ± 2[b]	109 ± 3	96 ± 2[a]	90 ± 6	93 ±12	99 ± 5	106 ± 3
HR	(beats/min)	420 ± 12	445 ± 13	394 ± 12	468 ± 7[a]	425 ± 13	436 ± 16	406 ± 11	421 ± 15
RR	(breaths/min)	134 ± 4	141 ± 5[b]	136 ± 2	155 ± 5[a]	145 ± 7	133 ± 8.0	151 ± 6	144 ± 5
Weight	(grams)	18 ± 0.4	18.4 ± 0.3	18.2 ± 0.4	18.4 ± 0.3	18.4 ± 0.4	17.7 ± 0.4	18.2 ± 0.4	18 ± 0.3

		Particle		Vehicle		Particle		Vehicle	
		Baseline	1 week	Baseline	1 week	Baseline	1 month	Baseline	1 month
MAP	(mmHg)	112 ± 5	102 ± 7[b]	109 ± 3	116 ± 3	96 ± 5	103 ± 7	80 ± 7	102 ± 6
HR	(beats/min)	420 ± 12	394 ± 16[b]	425 ± 12	451 ± 16	398 ± 22	426 ± 10	422 ± 14	437 ± 11
RR	(breaths/min)	134 ± 4	142 ± 12	136 ± 2	143 ± 8	121 ± 10	146 ± 5	138 ± 7	150 ± 7
Weight	(grams)	18.4 ± 0.4	17.8 ± 0.5	18.2 ± 0.4	17.9 ± 0.4	17.0 ± 0.6	20.0 ± 0.6[a]	17.5 ± 0.4	20.0 ± 0.4[a]

Table S2. Cardiovascular and biometric measurements. Thirty BALB/c mice (n=5 in Particle group and n=5 in Vehicle group for each time point) were IV injected with either anti-EpCAM Dynabeads (Particle) or saline (Vehicle), and the above measurements were taken before injection (baseline), immediately post-injection (t=0), and at 24 hours, 1 week, and 1 month post-injection. Values represent the mean ± SEM. The same group of mice was used for measurements at t=0 and at 1 week; thus, these time points are compared against the same baseline values. P-values were determined by 2-tailed Mann-Whitney nonparametric test. [a]Statistically significant difference (p-value <0.05) between time point and pre-injection baseline within the same experimental group; [b]Statistically significant difference (p-value <0.05) between Particle and Vehicle groups at a given time point. **MAP** = mean arterial pressure; **HR** = heart rate; **RR** = respiratory rate.

		24 hour		1 week		1 month		Reference
		Particle	Vehicle	Particle	Vehicle	Particle	Vehicle	Range
WBC	(K/µL)	6.1 ± 1.5	8.2 ± 0.2	4.5 ± 0.4	5.6 ± 0.4	6.1 ± 1.4	5 ± 0.5	5.7-14.8
RBC	(M/µL)	12 ± 0.3	12.2 ± 0.3	12.1 ± 0.2	13.2 ± 0.3	12.4 ± 0.5	12.9 ± 0.4	8.2-11.7
HGB	(g/dL)	18.2 ± 0.4	19 ± 0.5	18.6 ± 0.4 [a]	20.5 ± 0.6	19.2 ± 0.8	20.2 ± 0.6	12.4-18.9
HCT	(%)	54.2 ± 1.2	55.9 ± 1.2	56.4 ± 0.9	60.4 ± 1.4	57.5 ± 2.1	58.9 ± 1.4	43.5-67.0
MCV	(fL)	45.2 ± 0.4	45.7 ± 0.3	46.8 ± 0.3 [a]	45.7 ± 0.4	46.3 ± 0.1	45.5 ± 0.4	41.5-57.4 [b]
MCH	(pg)	15.4 ± 0.2	15.5 ± 0	15.4 ± 0.1	15.5 ± 0.1	15.5 ± 0.1	15.7 ± 0.2	13.0-17.6
MCHC	(g/dL)	34.1 ± 0.2	33.9 ± 0.2	32.9 ± 0.2 [a]	33.9 ± 0.2	33.4 ± 0.2	34.4 ± 0.5	30.5-34.2 [b]
Platelets	(K/µL)	928 ± 59	898 ± 112	827 ± 217	880 ± 92	738 ± 153	552 ± 105	476-1611
RDW	(%)	23.2 ± 0.4	23.3 ± 0.4	23.3 ± 0.3	24.7 ± 0.5	23.6 ± 0.7	24.3 ± 0.5	16.9-23.5
Reticulocytes	(%)	3.9 ± 0.3	4.6 ± 0.3	6 ± 0.1	6.1 ± 0.3	4.6 ± 0.1	4.6 ± 0.3	3.0-5.8 [b]
Neutrophils	(%)	6.4 ± 1 [a]	14.6 ± 3.1	15.6 ± 2.8	15.6 ± 7.2	13.4 ± 3.3	11.6 ± 1.5	10.4-27.9
Lymphocytes	(%)	87.2 ± 1.7 [a]	77.2 ± 1.6	76.8 ± 3.1	78.8 ± 7.7	79.2 ± 1.7 [a]	86.6 ± 1.4	65.0-87.0 [b]
Monocytes	(%)	6.4 ± 1.9	8 ± 1.9	7.2 ± 1	4.4 ± 1.2	6.4 ± 1.5	1.8 ± 0.7	3.8-14.3
Eosinophils	(%)	0 ± 0	0.2 ± 0.2	0.4 ± 0.2	1.2 ± 0.6	0.6 ± 0.4	0 ± 0	0.07-4.0
Basophils	(%)	0 ± 0	0 ± 0	0 ± 0	0 ± 0	0 ± 0	0 ± 0	0.0-1.6

		24 hour		1 week		1 month		Reference
		Particle	Vehicle	Particle	Vehicle	Particle	Vehicle	Range
AST	(U/L)	216 ± 42	151 ± 38	117 ± 9	170 ± 23	150 ± 13	151 ± 33	67-381
ALT	(U/L)	55.6 ± 13.9	43.8 ± 8.1	63.8 ± 23.3	67.4 ± 11.5	65.8 ± 11.5	42.4 ± 6.3	40-170
Alk Phos	(IU/L)	110 ± 5	107 ± 5.6	131 ± 10.2	129 ± 6	115 ± 4.1	113 ± 6.3	108-367
Cholesterol	(mg/dL)	109 ± 1.7	111 ± 3	98.2 ± 4.8	91.4 ± 5.2	104 ± 4	89.4 ± 12.7	81-208
BUN	(mg/dL)	20.2 ± 0.4	20.2 ± 1	17.6 ± 1.2	18 ± 0.3	16.8 ± 0.7	19.4 ± 2.1	7-31
Creatinine	(mg/dL)	0.05 ± 0.01 [a]	0.09 ± 0.01	0.08 ± 0.02	0.08 ± 0.02	0.18 ± 0.07	0.06 ± 0.04	0.1-1.1 [c]
T.Protein	(g/dL)	5.1 ± 0.1	5.1 ± 0.1	5.6 ± 0.1	5.4 ± 0.2	6 ± 0.3	6.6 ± 0.6	4.9-7.3
Albumin	(g/dL)	2.5 ± 0.5	2.4 ± 0.5	2.8 ± 0.1	2.6 ± 0.1	2.4 ± 0	2.9 ± 0.7	1.3-3.2 [b]
Sodium	(mmol/L)	151 ± 2	148 ± 0.4	148 ± 1.5	147 ± 0.5	147 ± 1 [a]	143 ± 0.4	130-172
Potassium	(mmol/L)	4.6 ± 0.1 [a]	5.5 ± 0.1	4.9 ± 0.2	5 ± 0.2	5.6 ± 0.3	5.8 ± 0.3	3.0-9.6 [c]
Chloride	(mmol/L)	109 ± 0.4 [a]	111 ± 0.2	111 ± 0.6	112 ± 0.7	109 ± 0.5	111 ± 0.6	101-139
Calcium	(mg/dL)	9.3 ± 0.1 [a]	9.7 ± 0.1	6.9 ± 0.1	7.3 ± 0.4	9.4 ± 0.1	8.6 ± 0.5	6.6-9.8 [b]
TIBC	(µg/dL)	- -	479 ± 20	401 ± 20	391 ± 6	431 ± 8	380 ± 28	N/A
Ferritin	(ng/mL)	706 ± 95	597 ± 30	546 ± 59	598 ± 76	725 ± 28	1036 ± 213	N/A
Total Iron	(µg/dL)	- -	230 ± 20	225 ± 28	276 ± 31	279 ± 14 [a]	225 ± 12	N/A

Table S3. Complete blood count and chemistry panel. BALB/c mice (n=5 per group) were IV injected with either anti-EpCAM Dynabeads (Particle) or saline (Vehicle), and the above hematological and biochemical measurements were taken at 24 hours, 1 week, and 1 month post-injection. Values represent the mean ± SEM. BALB/c clinical pathology reference ranges are from Charles River unless otherwise indicated. [a]Statistically significant difference (p-value <0.05) between Particle and Vehicle groups for the same time point. P-values were determined

by two-tailed Mann-Whitney nonparametric test. [b]Reference ranges adapted from Santos *et al*.[2]. [c]Stanford VSC Clinical Lab mouse reference value. **WBC**: white blood cells; **RBC**: red blood cells; **HGB**: hemoglobin; **HCT**: hematocrit; **MCV**: mean corpuscular volume; **MCHC**: mean corpuscular hemoglobin concentration; **AST**: aspartate transaminase; **ALT**: alanine transaminase; **Alk Phos**: alkaline phosphatase; **BUN**: blood urea nitrogen; **T. Protein**: total protein; **TIBC**: total iron-binding capacity.

Supplementary Notes

MP-labeling estimate

Our labeling estimate of 100 MPs per cell is conservative, given that 1) carcinoma cell lines commonly express > 100,000 EpCAM antigens per cell, with even low-EpCAM expressing cell lines still displaying > 1,000 antigens per cell[3], and 2) the maximum monolayer coverage of a 15 μm cell by 1 μm Dynabeads is approximately 1000 Dynabeads per cell, as described below. Additionally, microscopy of captured cells (**Fig. S9**) shows dense coverage of the majority of cells by Dynabeads. Furthermore, the magnetic force on a cell labeled with n MPs is equal to $n \times F_m$, so a 15 μm cell experiencing 15 times the drag force of a 1 μm MP requires labeling with only 15 MPs to be captured at the same rate. The surface area of a bead-labeled cell is described by $\pi(D_c + D_b)^2$, where D_c is the diameter of the cell and D_b is the diameter of the Dynabead. The cross-section of a Dynabead is $\frac{\pi {D_b}^2}{4}$. Assuming a hexagonal packing density of $\frac{\pi}{2\sqrt{3}}$, and the diameters stated above, the maximum number of Dynabeads that can occupy the cell surface is 929 beads, as expressed by $\frac{\pi^2(D_c+D_b)^2}{2\sqrt{3}} \times \frac{4}{\pi D_b^2} = \frac{2\pi}{\sqrt{3}}(\frac{D_c}{D_b} + 1)^2$.

Cells remain viable after magnetic enrichment

Ex-vivo culture of CTCs has been investigated as a promising tool for *in vitro* testing of drug susceptibility[4] but is currently only feasible for patients with high tumor burden and CTC counts - for example, one study required > 300 CTCs to create a colon cancer cell line[5]. Our method of magnetic enrichment can potentially capture manyfold more CTCs than a traditional blood draw, and may facilitate *ex-vivo* cell culture and drug susceptibility testing even in patients with a low tumor burden. To evaluate the effect of magnetic capture on cell viability, postlabeled cells

captured in blood were eluted and cultured without removing MPs from their surface. Untreated cells, along with cells prelabeled by MPs but not exposed to the MagWIRE, were grown for comparison. Cell proliferation measurements over 5 days revealed that MP-labeling had no effect on cell growth rate, and that the growth rate of cells captured with the MagWIRE was only slightly decreased in days 1-3 (**Fig. 3G**). Microscopy revealed a progressive decline in the level of MP cell coverage as cells divided and distributed the MPs to each daughter cell (**Fig. S9**). While these results are consistent with studies showing no measurable toxicity of MPs on cultured endothelial cells[6], the effect of bead binding and internalization on cellular activity should be minimized, and a number of techniques exist for dissociating magnetic beads from the cell surface[7]. Patient-derived CTCs will be more difficult to culture than cell lines, but our method of magnetic extraction does not appear to drastically affect viability, even when MPs remain attached to the recovered cells.

Gene expression profiling of captured cells

As further evidence for the downstream utility of CTCs captured with potentially disruptive magnetic gradients and forces, we performed targeted transcriptomic analysis of a set of 770 cancer-associated genes using the NanoString PanCancer Pathways Panel. Comparison of unperturbed, prelabeled, and MagWIRE captured H1650 cells revealed marked similarity in overall transcriptomic profiles even in a highly targeted gene set with concordance correlation coefficients of 0.9907 and 0.9832 for prelabeled and MagWIRE captured cells respectively. Cells that were captured by MagWIRE did exhibit statistically significant changes in ~4% of the genes analyzed at a false discovery rate of < 0.05, and nearly half of these genes (48%) exhibited a less than 2-fold change and nearly all (97%) exhibited a less than 3-fold change. Moreover, these genes were well distributed among a range of cell functions and signaling pathways

suggesting that these transcriptional changes are relatively non-specific. Furthermore, while we selected the 24-hour time point after MagWIRE capture to conduct the transcriptomic analysis to reveal relatively acute expression changes, it is possible that even these subtle alterations would subside at later time points as cells are allowed to recover in culture. For comparison, our correlation coefficients are similar to those seen with other immunomagnetic CTC isolation methods: cells captured with the MagSweeper, for example, showed correlation coefficients of 0.98-0.99, with the additional caveats that the MagSweeper expression profiling (1) was genome-wide rather than targeted to a fraction of cancer-specific cells, likely diluting any alterations; and (2) took place immediately after cell capture rather than 24 hours later, leaving little time for any transcriptomic changes to emerge[8].

We also profiled gene expression levels in unperturbed and MagWIRE-captured cells using an established system for single-cell transcriptomic analysis (Nanowell)[1]. Using a previously validated panel of genes that were shown to identify CTCs in NSCLC (MET, Vimentin (VIM), and aldehyde dehydrogenase (ALDH)), we observed marked similarity in patterns of expression for both MET (a proto-oncogene correlated with NSCLC progression) and VIM (an epithelial-mesenchymal transition marker) between unperturbed and MagWIRE captured cells. ALDH, a cancer stem cell marker, was noticeably downregulated in MagWIRE captured cells, potentially in response to cell stress. While "stemness" in particular may not affect the utility of CTC enumeration or drug susceptibility testing, this observation does argue for further investigation of which genes are susceptible to changes in expression with this method (and should thus not be used in transcriptomic analysis) as well as for how these transcriptomic alterations may resolve over time in culture.

EpCAM variability

Variation in EpCAM expression, both within and between cell passages, may contribute to the wide range of standard deviations observed in our capture efficiencies. Our flow cytometry analysis of H1650 cells agrees with previous studies[9] describing the relative heterogeneity of EpCAM expression (**Fig. S7A**), which could contribute to the variation in the degree of MP labeling that is seen on microscopy of labeled cells (**Fig. S7C, D, E**). Furthermore, the epithelial H1650 cell line has also been shown to contain mesenchymal subpopulations, which may evade EpCAM-based detection through EpCAM downregulation[10,11]. Although we used cells at a low passage number (< 10), we observed that cells at passage 10 contained large subpopulations of cells with mesenchymal morphology (**Fig. S7E, 6F**).

Cell numbers used for *in vivo* experiments

In our *in vivo* studies, we infused 2,500-10,000 cells into the auricular vein of a pig. Assuming a ~10 ml/min blood flow rate, which is a standard flow rate for a vein this size, our cell concentrations are 250-1,000 cells per mL. While these concentrations are at the high end of CTC concentrations seen clinically, we needed to inject sufficient CTCs during the short procedure time (just one minute) to minimize stochasticity in our capture measurements. Ideally, we would have liked to run the *in vivo* experiments for much longer to emulate the proposed clinical procedure, but outsourced MPs are too expensive for longer procedures. For future preclinical work, we therefore intend to synthesize our own MPs cheaply in-house.

Venous flow rate calculations

While Doppler ultrasound can be used to measure blood flow velocities in large arteries and veins, determining blood flow velocities in small veins is challenging. Therefore, we used literature estimates that correlate blood vessel size with average flow velocities. Based on the literature, blood flow velocities for ~2 mm diameter veins are typically in the range of 2-5

cm/sec[12]. The flow rate through a cylindrical vessel is given by $\pi r^2 v$, where r is the vessel radius and v is the flow velocity. For a 5 cm/sec (50 mm/sec) flow velocity in a 2 mm vessel, we obtain a flow rate of $\pi \times 1^2 \times 50 = 157$ mm^3/sec, or 9.4 mL/min.

Dose Calculations

For our *in vivo* study, we infused MPs intravenously at a rate of 2 mg/min, amounting to a total dose of 120 mg over an hour-long procedure. This is well below the standard dose of Feraheme (510 mg), an iron oxide nanoparticle formulation for the clinical treatment of iron deficiency anemia. For an average 70 kg adult, a 120 mg dose is equivalent to a dose per unit mass of 1.7 mg/kg. However, intravenous doses as high as 250 mg Fe/kg have been reported in rats without detectable symptoms or biochemical indicators of iron-induced toxicity[13-15]. In addition, the actual systemic exposure would be far less than 1.7 mg/kg because the MagWIRE magnetically captures a significant fraction of the injected MPs in their first pass by the wire.

MagWIRE saturation

As MPs and labeled cells accumulate on the surface of the MagWIRE, they occupy volume according to isosurfaces of magnetic energy density. The MagWIRE becomes 'saturated' when the occupied volume precludes new particles from accessing a volume of high magnetic gradient for capture. More importantly, the volume of accumulated particles must fit within the lumen of the catheter holding the MagWIRE during retrieval. For a catheter lumen that is 1.5 mm in diameter, the volume of particles that can accumulate on a 0.75 mm diameter MagWIRE and its sheath is 1.93×10^{10} μm^3. Assuming a dense sphere packing density of $\frac{\pi}{3\sqrt{2}}$, this volume corresponds to 2.72×10^{10} 1 μm MPs. The number of larger cells bound to the MagWIRE at physiologically relevant concentrations is negligible in comparison. Dynabeads contain about

10^9 particles per mg, so one MagWIRE can hold approximately 27 mgs of MPs. Thus, during a 1 hour infusion of 120 mg of MPs, the MagWIRE may be replaced 4-5 times.

Toxicity Study

Cardiovascular and Biometric Parameters

No qualitative changes were observed in appearance (e.g. fur, eyes, etc.), posture, gait, behavior, or social interactions during the month post-injection. MAP, HR, and RR immediately after injection showed a statistically significant difference from baseline in the vehicle group, but not in the particle group **(Table S2)**. These differences were relatively small and not physiologically significant. MAP and RR were statistically lower and higher, respectively, in the particle group than in the vehicle group immediately after injection, but the difference between the two groups was no longer statistically significant by 24 hours. MAP and HR were both statistically lower in the particle group than in the vehicle group at 1 week, but are within the ranges seen at baseline for other groups above. Mouse weight was statistically higher at 1 month compared to baseline in both particle and vehicle groups, as expected for young mice that are growing.

Complete Blood Counts

MCV and MCHC values at 1 week showed statistically significant differences between particle and vehicle groups of only 2.5% and 3%, respectively, but were within normal ranges **(Table S3)**. The hemoglobin values at 1 week showed statistically significant differences between particle and vehicle groups of ~9%, but the particle group was within the normal range. Hemoglobin values in vehicle groups at all time points and RBC counts across all groups were mildly elevated, possibly due to mild dehydration during overnight housing in metabolic cages. In the WBC differential, the lymphocyte fractions at 24 hours and 1 month were statistically higher and lower, respectively, in the particle group versus the vehicle group, but were within the

normal range. The neutrophil fraction was transiently low in the particle group at 24 hours, but was back within the normal range by 1 week. Acute neutropenia is often well tolerated and normalizes rapidly[16], but further studies will be needed to assess the trajectory of the neutropenia resolution during the first week post-injection.

Serum Chemistry Panel

Serum total iron was higher in the particle group than in the vehicle group at 1 month, but within the range of iron levels seen in the 1 week vehicle group **(Table S3)**. Notably, evidence of iron overload (e.g. elevated total iron and ferritin with decreased TIBC in particle vs. vehicle groups) was not observed at any time points. Sodium, potassium, and chloride values were all within published reference ranges for mice. Calcium levels were statistically lower in the particle group than in the vehicle group at 24 hours, but were still within the normal range. Creatinine levels at 24 hours were statistically lower in the particle group, but adverse effects on kidney health are associated with elevated (not lower) creatinine levels. Overall, hematological and biochemical parameters showed that most discrepancies between particle and vehicle groups were relatively minor. Even the moderate discrepancy in neutrophil fraction between particle and vehicle groups at 24 hours was no longer seen in subsequent time points.

Histological Findings

At each time point, there was variable accumulation of refractile, yellow to golden spherical bodies in the particle-treated animals. These spherical bodies measured approximately 1 μm in diameter and were present in various organs including the spleen and liver, to a much lesser degree in the lung and bone marrow, and rarely in the kidney and heart. In the liver, these

particles were associated with elongated cells along the hepatic cords (interpreted as perisinusoidal lining ["Ito"] cells). In the spleen, spherical bodies (which were distinct from the more amorphous, golden-brown hemosiderin deposits) were individualized, or present as small aggregates scattered throughout the red pulp (and minimally in the white pulp). In the lung, dense aggregates of spherical bodies were rarely present and associated with alveolar septal walls. Scattered in the bone marrow, spherical bodies were present as isolated particles, or in small clusters of generally 2-5 particles. Not all animals from the particle-treated groups had accumulations of these spherical bodies in the heart and kidney, but in the animals in which they were present, they were exceedingly rare and averaged one cluster per section. In the animals that had accumulations of spherical bodies, these accumulations were never associated with inflammation. Spherical bodies were not detected in any of the other organs examined in the particle-treated animals, and were never found in any organ of the vehicle-treated animals. In the particle-treated animals, the Perls' Prussian Blue stain highlighted large aggregates of spherical bodies, but generally failed to highlight smaller ones. In both the particle- and vehicle-treated animals, Perls' Prussian Blue highlighted hemosiderin deposits in the splenic red pulp. The Turnbull's blue reaction failed to highlight any material in the particle- or vehicle-treated animals. Both the Perls' Prussian Blue and the Turnbull's blue reaction highlighted deposits in positive control tissues. Overall, histology performed on the liver, spleen, lung, heart, kidney, bone marrow, and brain showed no adverse morphologic changes (no changes in tissue architecture, nor evidence of inflammation, necrosis, or immunologic derangements) to any of these organs over the one month period.

Biodistribution Study

Biodistribution studies showed that the injected MPs were predominantly taken up by the liver and spleen with a small amount of uptake by the lung. Average liver uptake from 24 hours to 1 month post-injection ranged from 68% to 95%, and average spleen uptake ranged from ~11% to 15% over this time period. The change in liver uptake between the 24 hour and 1 week time points, and between the 1 week and 1 month time points were not statistically significant. While the change in liver uptake between 24 hours and 1 month did reach significance, it is unlikely that this change reflects a true increase, especially as the levels in other organs (e.g. spleen) do not decrease. More likely, the apparent change may be attributable to the fact that the MP percent of injected dose for the liver is generalized from a portion of the organ, which may not accurately represent the distribution of MPs in the whole organ, leading to under- or overestimations of the true MP content. There was no change in spleen MP content over the course of the month. Lung uptake ranged from ~0.5% to 1%. Levels of MPs were below detectable limits in kidney, heart, bone marrow, and brain, as well as in urine and feces, at all timepoints. No MP signal was detected in organs from vehicle-treated mice. The fact that EPR signal did not decline in any of the organs in which signal was detectable suggests that one month is insufficient time for breakdown and clearance of these particles. Future studies will need to assess the biodistribution of MPs over much longer periods of time to determine whether the MPs are metabolized and eventually cleared from the mice. Past studies have shown that 10-30 nm iron oxide nanoparticles, such as those from which 1 μm Dynabeads are constituted, clear from the liver with half-lives of 3-4 weeks[17], so one might expect particles that are 30-100 fold larger to not have been broken down significantly at 30 days. However, despite retention of MPs, liver function tests (AST and ALT) were unaffected, suggesting that there was no functional impact on the liver.

Feasibility of capturing 100 nm MPs with the MagWIRE

An eventual goal of this work is to be able to use the MagWIRE in continuous flow mode *in vivo*, such that MPs are injected as a single bolus rather than a continuous infusion, especially for capture of smaller circulating biomarkers (ctDNA, exosomes, and proteins). While this is not possible with 1 μm MPs given their short circulation time ($t_{1/2}$ = 2.8 minutes), the use of smaller MPs (~100 nm), especially when PEGylated, can allow for much longer circulation times. However, a challenge of using smaller MPs is that magnetic moment scales with particle volume, and therefore the critical distance for capture is also smaller. While capture of 100 nm MPs is feasible, it requires optimization to be efficient; for example, by using MPs with higher saturation magnetization (M_s) and density, and wires that are longer and thicker. One hundred nanometer iron oxide MPs from MagSense Life Sciences have a density of 2.5 g/cm^3 and M_s of 60 emu/g according to their specification sheet, while online technical notes for MagSense MPs list their M_s at 130 emu/g (compared to Ms of ~20 emu/g and density of 1.7g/cm^3 for Dynabeads) due to their high iron oxide content (90%). We computationally simulated single-pass capture of one thousand 1 μm Dynabeads or 100 nm MagSense MPs (conservatively using the lower M_s of 60 emu/g) with a 0.74 mm-diameter MagWIRE to determine the number of MPs captured at various distances along the wire, up to 60cm (**Fig. S16A, B, D**). Our simulations show that the vast majority of 1 μm Dynabeads are captured within the first 5-10 cm of the wire, whereas 30 cm and 60 cm wires are required to capture 25% and 38%, respectively, of 100 nm MagSense MPs. Increasing the wire thickness to 1.56 mm, thereby halving the average distance from the wire surface to the lumen wall (0.82 mm to 0.41 mm), results in a capture efficiency of 72.4% and 95% at 30 cm and 60 cm, respectively, for 100 nm MagSense MPs (**Fig. S16C, D**). While a 60 cm wire length might be considered excessive for a superficial interventional

procedure, a wire length of 30 cm would still be within practical limits. However, it is important to note that these simulations are for single-pass capture. An advantage of using long-circulating MPs is that capture efficiencies can be increased further by increasing the intravascular dwell time of the wire, as MPs that are not captured on the first pass continue to circulate and can be captured on successive passes.

Theoretical framework for fast MP labeling of cells

Blood velocity in the pig ear vein is ~1-2 cm/sec. Therefore, the CTCs and MPs have only seconds to form complexes before being captured downstream by the MagWIRE. Complex formation between MPs and cells can be described by

$$[MP] + [CTC] \underset{k_{-1}}{\overset{k_1}{\rightleftharpoons}} [MP\text{-}CTC^*] \xrightarrow{k_2} [MP\text{-}CTC]$$

where k_1 and k_{-1} are the forward and reverse rate constants for the MP-CTC encounter complex, and k_2 is the forward rate constant for chemical fixation of an MP to a CTC, as for antibody-antigen kinetics[18]. Formation of the encounter complex is diffusion limited (e.g. $k_1 \approx \mathbf{k}_{diff}$), while chemical fixation is instantaneous by comparison ($k_2 >> k_1$). Due to the very high concentration of MPs (~10^8-10^9/mL) being infused, cells flowing through the infusion zone are in proximate contact (e.g. negligible diffusion distance) with a number of MPs to which they can instantaneously bind.

In addition to binding proximate MPs prior to reaching the MagWIRE, we believe that CTCs can bind a large number of MPs during passage over the wire. Specifically, as free MPs and CTCs start to flow over the MagWIRE and the wire magnetically attracts MPs, MPs start to move transverse to the direction of flow, crossing the trajectory of the CTCs and binding to the cells on

contact. This can greatly increase the number of MPs a CTC encounters, especially for cells that are closer to the wire. Thus, the forward rate constant changes from $k_1 \approx \mathbf{k}_{diff}$ before reaching the wire to $k_1 \approx \mathbf{k}_{mag}$ upon flowing over the wire, where k_{mag} is the magnetically-driven rate of mass transport of MPs towards the wire.

To illustrate the relative magnitudes of k_{mag} and k_{diff}, consider the rate of magnetic transport of MPs: Since >95% of MPs are captured by the wire in a single pass (~3 seconds), MPs that are furthest away from the wire (~1 mm) are traveling toward the wire at an average radial velocity of 0.33 mm/sec. This represents a <u>minimum</u> average radial velocity since MPs that are furthest away experience the weakest magnetic attraction. At this velocity, an MP that is 10 μm away from a CTC will reach the cell in 0.03 sec. By comparison, let us consider the diffusion rate of MPs: The diffusion coefficient (D_{MP}) is given by $D = kT/6\pi vR$, where k is the Boltzmann constant (1.38E-23 J/K), T is body temperature in Kelvin (310K), v is the viscosity of blood (3.2 mPa*s), and R is the MP radius (0.5μm). Thus, $D_{MP} = 0.142\ \mu m^2/sec$. The diffusion distance (x) for the MP is given by: $x^2 = 6D_{MP}t$. Therefore, an MP that is 10 μm away from a CTC will take ~117 seconds (nearly 2 minutes) on average to reach the cell by pure diffusion, illustrating that magnetic transport is ~3900-fold faster (0.03 sec vs. 117 sec) than diffusive transport over this distance. There is thus ample time for this magnetically-facilitated binding to occur even at flow velocities of 20 mL/min .

Supplementary Methods

NanoString gene expression analysis

H1650 cells that were either unperturbed, prelabeled, or postlabeled in a continuous flow experiment were cultured in RPMI medium for 24 hours to allow for emergence of potential transcriptomic alterations. Subsequently, RNA was extracted using a RNeasy Mini Kit (Qiagen, Hilden, Germany) and analyzed using the nCounter PanCancer Pathways Panel (NanoString Technologies, Seattle, WA) according to manufacturer instructions. Data were processed in nSolver Analysis Software version 4.0, using the Advanced Analysis version 2.0 add-on to assess pathways affected. Multiple hypothesis testing was controlled using the Benjamini-Yekutieli procedure with changes considered significant at a false discovery rate < 0.10.

Nanowell gene expression analysis

H1650 cells that were either unperturbed or postlabeled in a continuous flow experiment were cultured in RPMI medium for 24 hours to allow for emergence of potential transcriptomic alterations. Subsequently, cells were seeded in a Nanowell devices as previously described[1] to enable single-cell transcriptomic analysis of a previously validated NSCLC CTC identification panel (MET, ALDH, and VIM) using RT-PCR.

Evaluation of Particle Toxicity

Eight- to ten-week old immunocompetent female BALB/c mice (Charles River Laboratories) were maintained according to the guidelines of the Stanford University's Institutional Animal Care and Use Committee (Stanford, CA, USA). Sixty mice were randomly allocated to two different experimental groups (particle or vehicle). Pre-particle or pre-vehicle weights, vitals (heart rate, temperature, blood pressure and breathing rate) and observations on their physical appearance (e.g. fur, eyes, posture and gait), behavior and social interactions towards other mice

were recorded. Vitals (heart rate, temperature, blood pressure) were measured using a CODA surgical monitor (Kent Scientific Corporation). Via tail vein catheter, mice were intravenously administered 50µl particle (0.5mg) followed by a 50µl sterile saline flush (Particle Group, n=30) or 100µl sterile saline (Vehicle Group, n=30). For one cohort of mice (n=5 per experimental group), vitals and behavior were recorded immediately post particle/vehicle administration.

Five particle- and five vehicle-treated mice were euthanized at 24 hours, 1 week, and 1 month post-injection (n=30 mice total). A day prior to each time point, mice were placed in metabolic cages overnight to collect urine and feces. Final weights and vitals were also measured and observations of their physical appearance, behavior, and social interactions recorded. Following euthanasia, blood was collected for complete blood count (CBC) and urine was collected for measurement of specific gravity. Four of five mice from each group underwent necropsy and the harvested organs underwent pathologic evaluation and biodistribution studies. A separate cohort of thirty mice underwent terminal cardiac puncture at 24 hours, 1 week, and 1 month post-particle or vehicle administration (n=5 per timepoint per group), and the collected blood (~500 µL) was submitted to the Animal Diagnostic Lab at Stanford for serum chemistry analysis, including total iron, total iron binding capacity (TIBC), and ferritin.

Pathologic evaluation

Tissue samples collected for histology were fixed in 10% neutral buffered formalin (NBF), trimmed, routinely processed for paraffin embedding, and sectioned with a microtome. Serial sections were stained with hematoxylin and eosin (H&E), Perls' Prussian Blue (for ferric iron), and Turnbull's blue reaction (for ferrous iron). Tissues analyzed by light microscopy included liver, gallbladder, spleen, kidney, adrenal gland, pancreas, salivary glands, brain, cerebellum, heart, lung, trachea, esophagus, thyroid glands, thymus, long bone (including cortical bone and

bone marrow), and lymph nodes (cervical). Histologic analysis was performed by a veterinary pathologist blinded to the experimental groups.

Biodistribution of Magnetic Particles

For biodistribution studies, we analyzed MP uptake in liver, spleen, lung, heart, kidney, bone marrow, and brain. Whole organs were harvested at necropsy and weighed. Depending on size, either the entire organ or a tissue sample (also weighed) was transferred to saline buffer in a tube and mechanically homogenized. The tissue homogenates were then transferred to EPR tubes and frozen in liquid nitrogen for EPR studies. Percent injected dose in each organ was determined according to the following equation:

$$\% \text{ Injected Dose} = (EPR_{sample}/EPR_{standard}) \times (\text{Sample Volume}/\text{Standard Volume}) \times (\text{Mass of Organ}/\text{Mass of Tissue Sample})$$

wherein the standard contains the injected dose of MPs suspended in 300 uL of phosphate buffered saline.

Pharmacokinetics

Eight- to ten-week old immunocompetent female BALB/c mice were used to study the clearance of anti-EpCAM-conjugated 1-μm Dynabead MPs from the blood and determine the blood half-life of MPs. After administration of 0.5 mg MPs or saline vehicle via tail vein, blood was collected by terminal cardiac puncture over a range of time points post-injection: 1 min (n=4), 3 min (n=5), 5 min (n=3), 7.5 min (n=3) and 10 min (n=3). Blood was also collected from non-injected control mice (n=3). The blood was then transferred to EPR tubes and frozen in liquid nitrogen for EPR measurements of MP concentrations.

EPR Measurements and Data Analysis

X band EPR spectra were collected using a Bruker EMX spectrometer with an ER 041 XG microwave bridge and an ER4119HS sample cavity. X-band samples were run at 77 K using a liquid nitrogen finger dewar. EPR spectra were baseline corrected and integrated using the Xenon program (Bruker). X-band EPR settings were as follows: Freq ≈ 9.6 GHz, Power ≈ 2 mW, Rec. Gain = 10dB , Mod. Freq = 100 kHz, Mod. Amp. = 4.00G, Time Constant = 0.01ms, Conversion time = 1.00ms, Sweep Time = 64.0s.

Supplementary References

1. Park, S. *et al.* Molecular profiling of single circulating tumor cells from lung cancer patients. *Proc. Natl. Acad. Sci.* **113,** E8379–E8386 (2016).

2. Santos, E. W. *et al.* Hematological and biochemical reference values for C57BL/6, Swiss Webster and BALB/c mice. *Brazilian J. Vet. Res. Anim. Sci.* **53,** 138 (2016).

3. Rao, C. *et al.* Expression of epithelial cell adhesion molecule in carcinoma cells present in blood and primary and metastatic tumors. *Int. J. Oncol.* (2005). doi:10.3892/ijo.27.1.49

4. Stott, S. L. *et al.* Isolation of circulating tumor cells using a microvortex-generating herringbone-chip. *Proc. Natl. Acad. Sci. U. S. A.* **107,** 18392–7 (2010).

5. Cayrefourcq, L. *et al.* Establishment and Characterization of a Cell Line from Human Circulating Colon Cancer Cells. *Cancer Res.* **75,** 892–901 (2015).

6. Jackson, C. J., Garbett, P. K., Nissen, B. & Schrieber, L. Binding of human endothelium to Ulex europaeus I-coated Dynabeads: application to the isolation of microvascular endothelium. *J. Cell Sci.* **96 (Pt 2),** 257–62 (1990).

7. Clarke, C. & Davies, S. Immunomagnetic cell separation. *Methods Mol. Med.* **58,** 17–23 (2001).

8. Talasaz, A. H. *et al.* Isolating highly enriched populations of circulating epithelial cells and other rare cells from blood using a magnetic sweeper device. *Proc. Natl. Acad. Sci.* **106,** 3970–3975 (2009).

9. Shaw Bagnall, J. *et al.* Deformability-based cell selection with downstream immunofluorescence analysis. *Integr. Biol.* **8,** 654–664 (2016).

10. Yao, Z. *et al.* TGF- IL-6 axis mediates selective and adaptive mechanisms of resistance to molecular targeted therapy in lung cancer. *Proc. Natl. Acad. Sci.* **107,** 15535–15540 (2010).

11. Gorges, T. M. *et al.* Circulating tumour cells escape from EpCAM-based detection due to epithelial-to-mesenchymal transition. *BMC Cancer* **12,** 178 (2012).

12. Thiriet, M. *Biology and Mechanics of Blood Flows*. *CRM Series in Mathematical Physics* (Springer New York, 2008). doi:10.1007/978-0-387-74847-4

13. Bacon, B. R., Stark, D. D. & Park, C. H. Ferrite particles, a new MRI contrast agent: lack of acute or chronic hepatotoxicity following intravenous administration. *J Lab Clin Med* **110,** 164–171 (1987).

14. Arami, H., Khandhar, A., Liggitt, D. & Krishnan, K. M. In vivo delivery, pharmacokinetics, biodistribution and toxicity of iron oxide nanoparticles. *Chem. Soc. Rev.* **44,** 8576–8607 (2015).

15. Bakhtiary, Z. *et al.* Targeted superparamagnetic iron oxide nanoparticles for early

detection of cancer: Possibilities and challenges. *Nanomedicine Nanotechnology, Biol. Med.* **12,** 287–307 (2016).

16. Boxer, L. A. How to Approach Neutropenia. *ASH Educ. Progr. B.* **1,** 174–182 (2012).

17. Gu, L., Fang, R. H., Sailor, M. J. & Park, J.-H. In Vivo Clearance and Toxicity of Monodisperse Iron Oxide Nanocrystals. *ACS Nano* **6,** 4947–4954 (2012).

18. Galanti, M., D. Fanelli, and F. Piazza. Conformation-controlled binding kinetics of antibodies. *Scientific Reports*. **6**, 18976 (2016).